


Supersymmetric non-Hermitian topological interface laser

Motohiko Ezawa ¹, Natsuko Ishida,² Yasutomo Ota,³ and Satoshi Iwamoto²

¹*Department of Applied Physics, The University of Tokyo, 7-3-1 Hongo, Tokyo 113-8656, Japan*

²*Research Center for Advanced Science and Technology, The University of Tokyo, 4-6-1 Komaba, Tokyo 113-8656, Japan*

³*Research Center for Department of Applied Physics and Physico-Informatics, Keio University, 3-14-1 Hiyoshi, Japan*



(Received 22 October 2022; revised 15 January 2023; accepted 23 January 2023; published 9 February 2023)

We investigate laser emission at the interface of the topological and trivial phases in one dimension. The system is described by a generalized Su-Schrieffer-Heeger model with site-dependent hopping parameters involving the interface width parameter where gain (loss) is introduced only to the A (B) sites of the bipartite lattice. The topological interface state is described by the Jackiw-Rebbi state with a pure imaginary energy, reflecting the non-Hermiticity of the system. It feels only the gain effect since it is strictly localized at the A sites. The Jackiw-Rebbi state exists for any value of the interface width. We, thus, obtain a large area single-mode laser by making the interface width wide enough. We also find a series of analytic solutions of excited states based on supersymmetry (SUSY) quantum mechanics where the A and B sites of the bipartite lattice form SUSY partners. Furthermore, we study the system containing loss and gain with saturation by extending the Jackiw-Rebbi mode to a nonlinear theory.

DOI: [10.1103/PhysRevB.107.085302](https://doi.org/10.1103/PhysRevB.107.085302)

I. INTRODUCTION

Topological physics is one of the most exciting fields [1,2]. The Su-Schrieffer-Heeger (SSH) model is a simplest one-dimensional example of topological insulators [3]. The topological phase is characterized by the emergence of zero-energy states at the edges of a sample. A zero-energy state emerges also at an interface between a topological phase and a trivial phase, which is called a topological interface state. Topological photonics is an ideal playground of studying topological physics [4–21], where the system is non-Hermitian inevitably due to the presence of loss and gain [22,23]. The topological laser is one of the most successful applications of topological physics [24–41].

A high-power laser with high beam quality is important for applications. However, there is a limit of the power for a single laser due to the damage threshold. On the other hand, a multimode laser degrades the beam quality. In order to realize a large area single-mode laser, topological lasers are promising. There are several proposals on the single-mode laser using photonic crystals by using double-lattice photonic-crystal resonators [42], the accidental Dirac point [43,44], and Kekulé modulation [45,46] in the photonic lattice mostly over the past few years. Especially, it has been pointed out that a topological interface laser has enabled a large area single-mode lasing by using a smooth interface [47].

In this paper in order to study laser emission from the interface between topological and trivial phases, we analyze a non-Hermitian SSH model by including gain terms to the A sites and loss terms to the B sites of a bipartite system. The model is characterized by site-dependent hopping parameters. The topological interface state is described by the Jackiw-Rebbi (JR) state [48], which is a mode formed only on the A

sites. The JR state exists for any value of the interface width, indicating that a large area single-mode laser is possible by taking the interface width wide enough. We also find a series of analytic solutions of excited states making supersymmetry (SUSY) partners based on SUSY quantum mechanics where the JR state is the ground state.

This paper is composed as follows. In Sec. II, we introduce a generalized SSH model by including gain terms with parameter $\gamma\chi$ to the A sites and loss terms with parameter γ to the B sites. The hopping interaction is characterized by site-dependent hopping parameters involving a dimensionless interface width parameter ξ .

In Sec. III, we investigate the linear model by neglecting the saturation effect. The model is a non-Hermitian SSH model, whose energy is complex. Provided the interface width is sufficiently narrow ($\xi \rightarrow 0$), the standard topological analysis is applicable, leading to the emergence of the topological interface state according to the bulk-edge correspondence. We examine what happens when we increase ξ . We confirm numerically that the interface state is generated at any value of ξ . We also apply quench dynamics to investigate the dynamics of a topological interface laser.

In Sec. IV, by taking a continuous approximation of the model, we obtain the JR solution describing the interface state. It has a pure imaginary energy, reflecting the non-Hermiticity of the system. The solution exists for any value of ξ in accord with the numerical results derived in Sec. III. The JR mode is strongly enhanced because it is strictly localized at the A sites and has the largest imaginary eigenvalue. The strength of single-mode lasing becomes stronger for larger ξ . We, thus, obtain a large area single-mode laser with a wide interlayer width.

In Secs. V and VI, we argue that sSUSY quantum mechanics underlies the basic structure of the present bipartite system. By extending SUSY quantum mechanics to non-Hermitian systems, we find a series of analytic solutions formed either A or B sites where the JR state is the ground state. Here, SUSY partners are formed on the A and B sites, which we call SUSY JR modes. Not only the topological interface state, but also the SUSY JR modes are shown to have pure imaginary energies. We confirm that the analytical solutions well coincide with numerical solutions.

In Sec. VII, we include a saturation term to the gain, which is a nonlinear term. Such a system well describes a large area single-mode laser emission from an interface of a topological system. We extend the JR mode to the nonlinear regime. Excitations at B sites are induced in the JR mode by a nonlinear effect where the wave function at B sites is fixed to be pure imaginary. The relative phases between the saturated wave functions at the A and B sites are fixed. Furthermore, it is shown that bulk modes emerge in transient process but decay eventually. Namely, the JR topological mode is solely stimulated in stable laser emission. Since the JR mode extends over a wide region around the interface, it gives a large area single-mode topological laser even if the saturation term is present.

Section VIII is devoted to the conclusion and a discussion. Appendices are prepared for a review of the topological property of the non-Hermitian SSH model and for a detailed analysis of nonlinear JR solutions. We also derive the generalized SSH model we have employed from a more basic theory, that is the rate equation.

II. MODEL

We investigate the dynamics of a laser system governed by [26]

$$i \frac{d\psi_n}{dt} = \sum_{nm} M_{nm} \psi_m - i\gamma \left(1 - \chi \frac{[1 - (-1)^n]/2}{1 + |\psi_n|^2/\eta} \right) \psi_n, \quad (1)$$

with a site-dependent hopping matrix,

$$M_{nm} = \kappa_{A,n} (\delta_{2n,2m-1} + \delta_{2m,2n-1}) + \kappa_B (\delta_{2n,2m+1} + \delta_{2m,2n+1}), \quad (2)$$

where ψ_n is the amplitudes at the site n , where $n = 1, 2, \dots, N$ in the system composed of N sites; γ represents the loss in each resonator; χ represents the amplitude of the optical gain via stimulated emission induced only at the odd site; η represents the saturation parameter [26]. All these parameters are taken positive semidefinite. The lattice structure of the SSH model is bipartite where the odd and even sites are called the A and B sites, respectively. The system turns out to be a linear model in the limit $\eta \rightarrow \infty$. On the other hand, γ controls the non-Hermiticity where the system is Hermitian for $\gamma = 0$. In Eq. (1) we measure time t in units of $1/\kappa$ and the loss parameter γ in units of κ , where κ is defined in Eq. (3) just below. Furthermore, we set $\kappa = 1$ in numerical studies.

The hopping parameter $\kappa_{A,n}$ has a site dependence, whereas κ_B does not. They are given by

$$\kappa_{A,n} = \kappa \left(1 + \lambda \tanh \frac{n - n_{\text{IF}} + 1/2}{\xi} \right), \quad \kappa_B = \kappa, \quad (3)$$

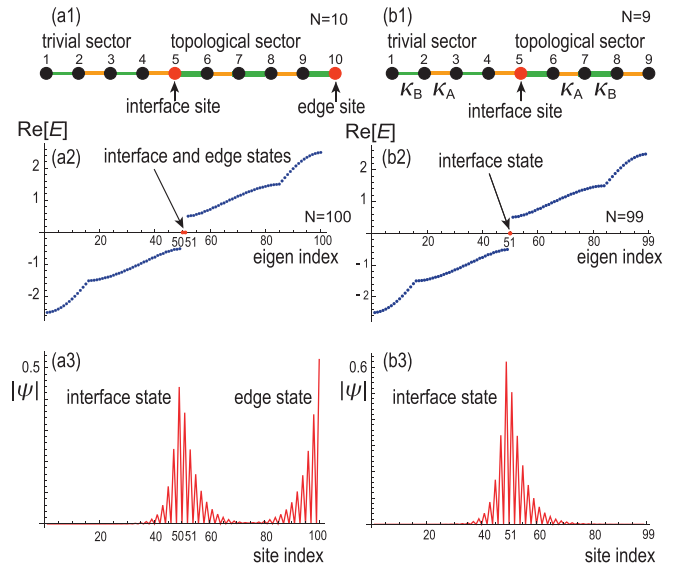


FIG. 1. (a1) and (b1) Illustration of the interface (marked in red) in the SSH chain for $N = 10$ and 9 . (a1) Topological edge states (marked in red) appear at the two edges of a topological sector. (b1) The topological edge state is absent at the edge of a chain when N is odd. The topological state emerges only at the interface. (a2) and (b2) Energy spectrum (vertical axis) of the SSH model as a function of the eigenindex (horizontal axis) for $N = 100$ and 99 where the eigenindex is sorted in the increasing order of the energy. Two and one zero-energy topological states (marked in red) emerge in the SSH chain with $N = 10$ and 9 . The structure of kinks at $p = 16$ and $p = 84$ is due to the difference of the bandwidth between the topological and the trivial sectors. (a3) The spatial profile of the absolute value of the eigenfunctions corresponding to the interface and edge states, which are twofold degenerated. (b3) The spatial profile of the absolute value of the interface state. We have set $\xi = 1$ and $\lambda = 0.5$.

where $\lambda > 0$ and $\xi > 0$ represent the interface modulation and the interface width, respectively. Small (large) ξ represents a sharp (smooth) interface. n_{IF} is the smallest odd number larger than or equal to $N/2$. Then, $n - n_{\text{IF}} + 1/2 > 0$ for $n \geq n_{\text{IF}}$, and $n - n_{\text{IF}} + 1/2 < 0$ for $n < n_{\text{IF}}$. We call the site $n = n_{\text{IF}}$ the interface of the chain. See Figs. 1(a1) and 1(b1) for an illustration in the case of $N = 10$ and 9 .

The explicit equations for a finite chain with length N follow from Eq. (1) as

$$i \frac{d\psi_{2n-1}}{dt} = \kappa_B \psi_{2n-2} + \kappa_{A,n} \psi_{2n} - i\gamma \left(1 - \frac{\chi}{1 + |\psi_{2n-1}|^2/\eta} \right) \psi_{2n-1}, \quad (4)$$

$$i \frac{d\psi_{2n}}{dt} = \kappa_B \psi_{2n+1} + \kappa_{A,n} \psi_{2n-1} - i\gamma \psi_{2n}. \quad (5)$$

We solve this set of equations together with the initial condition,

$$\psi_n(t = 0) = \delta_{n, n_{\text{IF}}}. \quad (6)$$

This is quench dynamics starting from the interface site by giving an input to it initially. The initial input triggers the gain effect in Eq. (4) because n_{IF} is an odd number.

A comment is in order. When we scale the amplitude as $\psi_n(t) = \sqrt{\eta}\psi'_n(t)$, the parameter η disappears from the equations of motion (4) and (5). It appears in the initial condition (6) instead. However, we use the amplitude $\psi_n(t)$ in what follows since it is convenient to use η to control the nonlinearity of the model.

III. LINEAR THEORY

We start with the linear model ($\eta \rightarrow \infty$). Then, Eq. (1) is reduced to

$$i\frac{d\psi_n}{dt} = \sum_{nm} M_{nm}\psi_m - i\gamma\{1 - \chi[1 - (-1)^n]/2\}\psi_n, \quad (7)$$

or

$$i\frac{d\psi_n}{dt} = \sum_m \tilde{M}_{nm}\psi_m, \quad (8)$$

where

$$\tilde{M}_{nm} = \bar{M}_{nm} - i\gamma\left(1 - \frac{\chi}{2}\right)\delta_{nm}, \quad (9)$$

with

$$\bar{M}_{nm} = M_{nm} - i\gamma\chi\frac{(-1)^n}{2}\delta_{nm}. \quad (10)$$

Hereafter, we use \tilde{M}_{nm} for the study of dynamics and \bar{M}_{nm} for the analytical study of the system. Since \tilde{M}_{nm} and \bar{M}_{nm} are different only by a c -number term, they describe an identical non-Hermitian SSH model with gain and loss where hopping parameters have a site dependence as described by Eq. (3).

A. Topological edge and interface states

1. SSH model

We analyze the SSH model M_{nm} in the case of a sharp interface ($\xi \rightarrow 0$). Then, Eq. (3) amounts to

$$\begin{aligned} \kappa_{A,n} &= \kappa(1 + \lambda) & \text{for } n \geq n_{\text{IF}}, \\ \kappa_{A,n} &= \kappa(1 - \lambda) & \text{for } n < n_{\text{IF}}. \end{aligned} \quad (11)$$

The hopping amplitudes are constant $\kappa_{A,n} = \kappa(1 + \lambda)$ for the segments with $n \geq n_{\text{IF}}$, whereas they are constant $\kappa_{A,n} = \kappa(1 - \lambda)$ for the segments with $n < n_{\text{IF}}$, separately. Note that $\kappa_B = \kappa$. The hopping matrix M_{nm} defines the SSH model in each segment.

The SSH model with constant hopping amplitudes κ_A and κ_B has a topological phase for $\kappa_A < \kappa_B$ and the trivial phase for $\kappa_A > \kappa_B$. The topological phase is characterized by the emergence of zero-energy states at the both edges of a finite chain as demonstrated numerically in Fig. 1(a2) for $N = 100$. This is the standard bulk-edge correspondence. It is illustrated in Fig. 1(a1) for $N = 10$. See Appendix A for details.

There is an intriguing phenomenon in the SSH model with respect to the even-odd effect of the number of the sites within the chain [38,47]. We may remove the edge site at $n = N$ from an SSH chain with even N to obtain an SSH chain with odd total number $N - 1$. See an illustration in Figs. 1(a1) and 1(b1) where two chains with $N = 10$ and 9 are shown. We demonstrate numerically that there is only one zero-mode state in the odd chain with $N = 99$ in Fig. 1(b2), which is

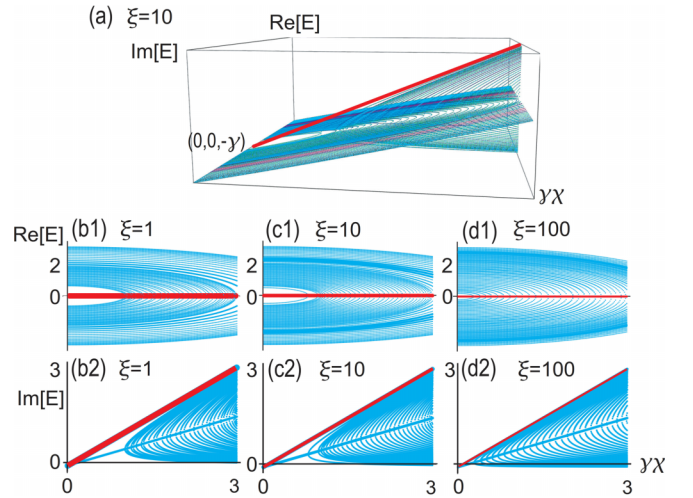


FIG. 2. (a) Energy spectrum in the $(\gamma\chi, \text{Re}[\tilde{E}], \text{Im}[\tilde{E}])$ space for $\xi = 10$, where $\gamma\chi$ stands for the gain ($0 < \gamma\chi < 1.5$). (b1), (c1), and (d1) Energy spectrum in the $(\gamma\chi, \text{Re}[\tilde{E}])$ plane for $\xi = 1, 10, 100$. (b2), (c2), and (d2) Energy spectrum in the $(\gamma\chi, \text{Im}[\tilde{E}])$ plane for $\xi = 1, 10, 100$ by fixing $\gamma = 0.1$. The red line represents the topological interface state, whose energy is pure imaginary. The width of the line is proportional to the local density of states. The interface state is well separated from (almost touched to) the bulk spectrum for $\xi = 1, 10$ ($\xi = 100$). We have set $\gamma = 0.1$ and $\lambda = 0.5$. We have used the chain with $N = 99$.

the topological interface state illustrated in Fig. 1(a2). This is also a bulk-edge correspondence. Recall that the topological number is defined for the unit cell of the bulk.

We have displayed the eigenfunctions in Figs. 1(a3) and 1(b3) for the case of $N = 100$ and $N = 10$ where they are found to be quite broad.

In the rest of this paper, we focus on the topological interface state by taking an SSH chain with odd N . Strictly speaking, the topological numbers are well defined only in the limit $\xi \rightarrow 0$. However, we are actually interested in systems having a very smooth interface ($\xi \approx N$) to create a high-power laser. We investigate how the topological interface state behaves as a function of ξ . We demonstrate numerically that it persists even for $\xi \approx N$. This is because the interface state is actually the JR state associated with a smooth interface for any value of ξ , whose stability is guaranteed as far as the hopping modulation forms a domain wall structure as we argue in Sec. VI.

2. Non-Hermitian SSH model

We investigate the system \tilde{M}_{nm} with a finite loss ($\gamma \neq 0$) and gain ($\gamma\chi \neq 0$). Diagonalizing the hopping matrix \tilde{M}_{nm} in Eq. (9) numerically, we obtain the energy spectrum \tilde{E} as a function of χ whereas setting $\gamma = 0.1$. We show the results in the $(\chi, \text{Re}[\tilde{E}], \text{Im}[\tilde{E}])$ space for $\xi = 10$ in Fig. 2(a). See also Figs. 2(c1) and 2(c2) for its cross section at $\text{Im}[\tilde{E}] = -\gamma$ and $\text{Re}[\tilde{E}] = 0$, respectively. It means that the systems is lossy for $\chi = 0$. We clearly observe a straight line passing through the point $(0, 0, -\gamma)$ in the $(\chi, \text{Re}[\tilde{E}], \text{Im}[\tilde{E}])$ space, which represents the energy of the topological interface state we have just discussed.

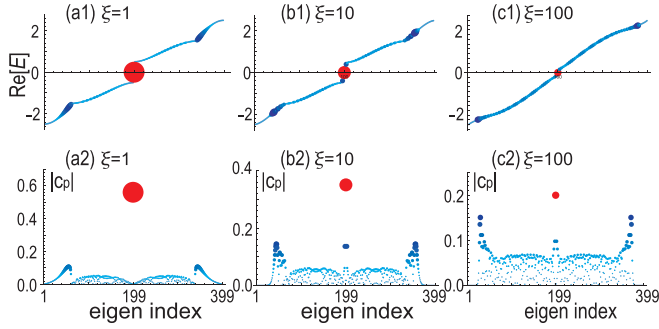


FIG. 3. (a1), (b1), and (c1) Real part of energy E_p and (a2), (b2), and (c2) the component $|c_p|$ as functions of the eigenindex p . A red large disk indicates the topological interface state. On the other hand, cyan small disks indicate the bulk states. The size of a disk is proportional to the local density of states. It becomes smaller for larger ξ because the interface mode becomes broader. The horizontal axis is the eigenindex. (a1) and (a2) $\xi = 1$; (b1) and (b2) $\xi = 10$; (c1) and (c2) $\xi = 100$. We have set $N = 399$, $n_{\text{IF}} = 199$, and $\gamma = 0$.

Similarly, we show the energy spectrum for $\xi = 1$ and 100 in Figs. 2(b1), 2(b2), 2(d1), and 2(d2). We also find a straight line passing through the point $(0, 0, -\gamma)$ in the $(\chi, \text{Re}[\tilde{E}], \text{Im}[\tilde{E}])$ space.

The energy of the topological interface state is well fitted for any system parameters by the formula,

$$\bar{E}_{\text{IF}} = i\bar{\gamma} \quad \text{with} \quad \bar{\gamma} = \gamma\chi/2. \quad (12)$$

The eigenvalue (12) and the associated eigenfunction are derived as a JR solution later in Sec. IV: See Eq. (30).

Furthermore, we observe a band-edge mode [47] between the interface mode and the bulk spectrum for $\xi = 10$. In the case of $\xi = 100$, in addition to the band-edge mode, there are many modes with almost equal spacing and characterized by their pure imaginary energies. We call them SUSY JR modes with respect to which we discuss based on the SUSY quantum mechanics in Sec. VI: See the energy spectrum in Eq. (57).

B. Dynamics

The quench dynamics is a powerful tool to distinguish topological phase even for nonlinear systems [49–52]. Before analyzing the dynamics of the system, it is convenient to study the eigenvalues and the eigenfunctions of the hopping matrix \tilde{M}_{nm} given by Eq. (9). We diagonalize it as

$$\tilde{M}\phi_p = \tilde{E}_p\phi_p, \quad (13)$$

where an integer p labels the eigenindex, $1 \leq p \leq N_2$ and ϕ_p is the eigenfunction. We show the eigenvalues \tilde{E}_p in Figs. 3(a1)–3(c1). Let the wave function of the topological interface state be ϕ_{IF} . Its eigenvalue is

$$\tilde{E}_{\text{IF}} = \bar{E}_{\text{IF}} - i\gamma\left(1 - \frac{\chi}{2}\right)\delta_{nm} = i\gamma(\chi - 1), \quad (14)$$

with the use of Eqs. (9) and (12).

Decoupled equations follow from Eq. (8) for the eigenfunctions,

$$i\frac{d\phi_p}{dt} = \tilde{E}_p\phi_p, \quad (15)$$

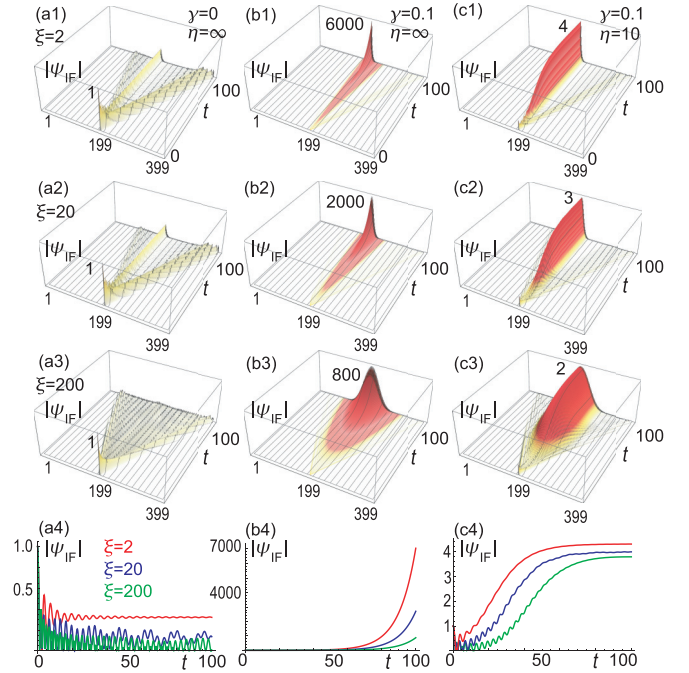


FIG. 4. (a1)–(c1), (a2)–(c2), and (a3)–(c3) Time evolution of the spatial profile for the time interval $0 < t < 100$ and (a4)–(c4) that of the amplitude $|\psi_{\text{IF}}|$ at the interface for the time-interval $0 < t < 100$ for various penetration depth ($\xi = 2$, $\xi = 20$, $\xi = 200$). (a1)–(c1) Hermitian model ($\gamma = 0$). (b1)–(b3) Linear non-Hermitian model ($\gamma = 0.1$, $\chi = 2$, $\eta = \infty$). (c1)–(c3) Nonlinear non-Hermitian model ($\gamma = 0.1$, $\chi = 2$, $\eta = 10$). We have set $N = 399$, where $n_{\text{IF}} = 199$.

whose solutions are given by

$$\phi_p(t) = \exp[-it\tilde{E}_p]\phi_p. \quad (16)$$

In particular, for the topological interface state, we have

$$\phi_{\text{IF}}(t) = \exp[\gamma(\chi - 1)t]\phi_{\text{IF}}, \quad (17)$$

with the use of Eq. (14). It has no dynamics for $\gamma = 0$ or $\chi = 1$. On the other hand, it grows exponentially for $\chi > 1$.

The initial state (6) is expanded in terms of the eigenfunctions as

$$\psi_n(t=0) = \delta_{n,n_{\text{IF}}} = \sum_p c_p\phi_p. \quad (18)$$

We show the coefficient $|c_p|$ in Figs. 3(a2)–3(c2), which is determined by

$$c_p = \sum_n \delta_{n,n_{\text{IF}}}\phi_p. \quad (19)$$

It is the overlap between the initial state (6) and the eigenstate ϕ_p . Such an overlap for the topological interface ϕ_{IF} is $|c_{\text{IF}}|$, which is found large for $\xi = 1$ but small for $\xi = 100$ in Fig. 3. This is because the topological interface state is strictly localized at the interface for small ξ but broad for large ξ .

We now investigate the quench dynamics of the system by imposing the initial condition (6).

First, we neglect the loss and gain terms by setting $\gamma = 0$. We numerically solve a set of differential equations (4) and (5), whose results are shown in Figs. 4(a1)–4(a3). The input given initially at the site $n = n_{\text{IF}}$ spreads over the chain, but

the component $|c_{\text{IF}}|$ remains as it is because $\phi_{\text{IF}}(t) = \phi_{\text{IF}}$ in Eq. (17) for $\gamma = 0$. There is a peak at the interface for $\xi = 2$ as in Fig. 4(a1) but the peak is tiny for $\xi = 200$ as in Fig. 4(a3).

Second, we include the linear loss and gain terms ($\gamma\chi \neq 0$), whose results are shown in Figs. 4(b1)–4(b3). The topological interface state has a maximum value at the site with gain. As a result, the state exponentially evolves and becomes infinite. However, this is not physical. Indeed, there is a saturation of the gain in actual experiments, about which we discuss in Sec. VII. It is a saturation effect ($\eta < \infty$). Here, we present the results in Figs. 4(c1)–4(c3) by choosing $\eta = 10$.

We show the time evolution of the amplitude $|\psi_{m\text{IF}}|$ in Figs. 4(a4)–4(c4). It becomes stationary after a certain time in the absence of the loss and gain terms ($\gamma = 0$) as shown in Fig. 4(a4). On the other hand, the amplitude exponentially becomes large once the loss and gain terms are present ($\gamma\chi \neq 0$) as shown in Fig. 4(b4). It becomes stationary by the saturation term ($\eta < \infty$) as in Fig. 4(c4), about which we discuss in Sec. VII.

IV. JACKIW-REBBI SOLUTION IN THE NON-HERMITIAN MODEL

Supersymmetric quantum mechanics is a method to obtain an analytic solution originally proposed by Witten [53]. See also Refs. [54–56] for reviews. It has also been applied to laser systems [57–62].

We continue to study the linear model but based on the parity-time- (PT-)symmetric non-Hermitian SSH model \bar{M}_{nm} from now. The two matrices \tilde{M}_{nm} and \bar{M}_{nm} are different only by a c number as in Eq. (10). Hence, the eigenfunctions are identical with the eigenvalues different only by this c number.

We diagonalize the matrix \bar{M}_{nm} by employing an approximation similar to the one made by Jackiw and Rebbi. The hopping amplitude (3) becomes constant as in Eq. (11) far away from the interface. Then, the hopping matrix \bar{M}_{nm} can be presented in the momentum space as

$$\bar{H} \equiv \begin{pmatrix} i\bar{\gamma} & \kappa_A + \kappa_B e^{-iak} \\ \kappa_A + \kappa_B e^{iak} & -i\bar{\gamma} \end{pmatrix}. \quad (20)$$

The energy spectrum reads

$$\bar{E}(k) = \pm \sqrt{\kappa_A^2 + \kappa_B^2 + 2\kappa_A\kappa_B \cos ak - \bar{\gamma}^2}, \quad (21)$$

which has a Dirac-like dispersion in the vicinity of the momentum $k = \pi/a$. Assuming a sufficiently smooth configuration in the vicinity of $k = \pi/a$, we expand it as

$$\bar{H} = \begin{pmatrix} i\bar{\gamma} & \Delta_0 + i\kappa k' \\ \Delta_0 - i\kappa k' & -i\bar{\gamma} \end{pmatrix}, \quad (22)$$

with

$$\Delta_0 = \kappa_A - \kappa_B, \quad k' = k - \pi. \quad (23)$$

We bring back this Hamiltonian to the continuous coordinate space as

$$\bar{H} = \begin{pmatrix} i\bar{\gamma} & \Delta(x) - \kappa\partial_x \\ \Delta(x) + \kappa\partial_x & -i\bar{\gamma} \end{pmatrix} = \begin{pmatrix} i\bar{\gamma} & A^\dagger \\ A & -i\bar{\gamma} \end{pmatrix}, \quad (24)$$

with

$$A \equiv \Delta(x) + \kappa\partial_x, \quad A^\dagger \equiv \Delta(x) - \kappa\partial_x, \quad (25)$$

and

$$\Delta(x) = \kappa\lambda \tanh \frac{x - x_{\text{IF}}}{a\xi}, \quad (26)$$

where we have recovered the site-dependent hopping amplitude from Eq. (3).

The eigenvalue equation of the Hamiltonian for the p -th eigenindex (24) reads

$$\bar{H} \begin{pmatrix} \Psi_p^A(x) \\ \Psi_p^B(x) \end{pmatrix} = \bar{E}_p \begin{pmatrix} \Psi_p^A(x) \\ \Psi_p^B(x) \end{pmatrix}, \quad (27)$$

with (24), where we have defined the wave functions with the eigenvalue \bar{E}_p at the A and B sites as $\Psi^A(x)$ and $\Psi^B(x)$, respectively.

We derive the eigenfunction representing the topological interface state. Its eigenenergy \bar{E}_{IF} is given by Eq. (12) in the \bar{M}_{nm} basis, which reads $\bar{E}_{\text{IF}} = i\bar{\gamma}$ in the \bar{H} basis. Hence, Eq. (27) yields

$$\bar{H} \begin{pmatrix} \Psi_0^A(x) \\ \Psi_0^B(x) \end{pmatrix} = i\bar{\gamma} \begin{pmatrix} \Psi_0^A(x) \\ \Psi_0^B(x) \end{pmatrix}, \quad (28)$$

with $\bar{E}_0 = \bar{E}_{\text{IF}} = i\bar{\gamma}$ and (24) for \bar{H} . It is easy to obtain one solution by setting $\Psi_0^B(x) = 0$. The equation for $\Psi^A(x)$ reads

$$A\Psi_0^A(x) = [\Delta(x) + \kappa\partial_x]\Psi_0^A(x) = 0, \quad (29)$$

for which the JR solution follows:

$$\Psi_0^A(x) = c \exp \left[-\frac{1}{\kappa} \int^x \Delta(x') dx' \right], \quad (30)$$

$$\Psi_0^B(x) = 0, \quad (31)$$

with c is a normalization constant. This is a non-Hermitian generalization of the JR mode with a pure imaginary eigenvalue. It is the unique solution because there is no degeneracy in the topological interface state.

The solution (30) is a simple functional of the hopping function $\Delta(x)$ given by Eq. (26). There are several key features. (1) The solution exists for any value of the interface width parameter ξ . (2) We may use it for a sample with an arbitrary size. (3) The solution does not depend on the precise form of the hopping function $\Delta(x)$. The crucial requisite is that the sign of the hopping function (26) has opposite signs between the right- and the left-hand sides of the chain, i.e.,

$$\Delta(x) > 0 \quad \text{for } x > x_{\text{IF}} \quad \text{and} \quad \Delta(x) < 0 \quad \text{for } x < x_{\text{IF}}. \quad (32)$$

Then, a domain-wall-type solution is necessarily generated around $x = x_{\text{IF}}$. This is the JR solution. Its stability is assured as far as the condition (32) is satisfied.

The JR mode has the largest imaginary eigenvalue as in Fig. 2(b2). It is understood as follows. As we will soon see, the JR mode has amplitude only at the A sites to which the gain is introduced. On the other hand, the other modes have amplitudes both at A and B sites. Namely, the JR mode feels only the gain effect but the other modes feel both gain and loss effects. Hence, the JR mode has the largest positive imaginary energy, which means that it feels the largest gain effect.

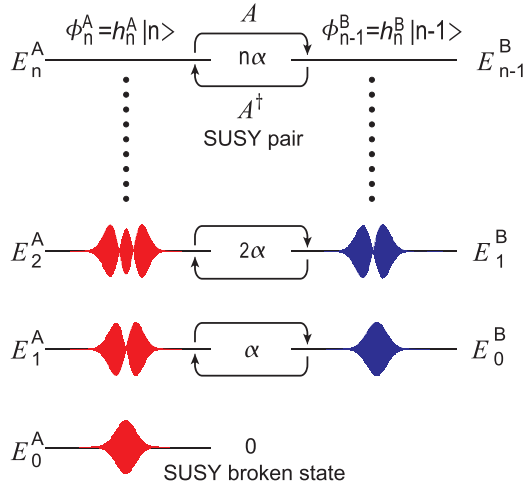


FIG. 5. Illustration of the energy levels and the SUSY quantum mechanics. Wave functions are shown in the case of $h_n^A = h_n^B$ for the Hermitian system.

V. SUSY QUANTUM MECHANICS

When an operator A is given, we may define the supercharges Q , Q^\dagger and the Hamiltonian \hat{H} by [53–56]

$$Q \equiv \begin{pmatrix} 0 & 0 \\ A & 0 \end{pmatrix}, \quad Q^\dagger \equiv \begin{pmatrix} 0 & A^\dagger \\ 0 & 0 \end{pmatrix}, \quad (33)$$

$$\hat{H} = \{Q, Q^\dagger\} = \begin{pmatrix} A^\dagger A & 0 \\ 0 & AA^\dagger \end{pmatrix}. \quad (34)$$

The superalgebra follows:

$$\{Q, Q\} = \{Q^\dagger, Q^\dagger\} = [\hat{H}, Q] = [\hat{H}, Q^\dagger] = 0. \quad (35)$$

A representation of the algebra is constructed as follows:

We define the operators

$$H_A \equiv A^\dagger A, \quad H_B \equiv AA^\dagger. \quad (36)$$

The eigenvalue equations are

$$H_A \phi_p^A = E_p^A \phi_p^A, \quad H_B \phi_p^B = E_p^B \phi_p^B. \quad (37)$$

Using these we obtain

$$H_B(A\phi_p^A) = AA^\dagger A\phi_p^A = E_p^A(A\phi_p^A), \quad (38)$$

$$H_A(A^\dagger\phi_p^B) = A^\dagger AA^\dagger\phi_p^B = E_p^B(A^\dagger\phi_p^B), \quad (39)$$

and, hence, $A\phi_p^A$ is an eigenstate of H_B with the eigenvalue E_p^A . If we assume $E_0^A = 0$ and $E_0^B \neq 0$, we may choose $q = p + 1$. Then, $\phi_p^B(x) \propto A\phi_{p+1}^A(x)$ and $\phi_{p+1}^A(x) \propto A^\dagger\phi_p^B(x)$ so that

$$E_p^B = E_{p+1}^A, \quad E_0^A = 0. \quad (40)$$

The wave functions give a representation of the SUSY algebra as illustrated in Fig. 5.

We now show that the present model presents a non-Hermitian representation of the SUSY algebra. We may use Eq. (25) for A and A^\dagger . For the Hamiltonian (24) we find

$$\bar{H}^2 = \begin{pmatrix} -\bar{\gamma}^2 + A^\dagger A & 0 \\ 0 & -\bar{\gamma}^2 + AA^\dagger \end{pmatrix}. \quad (41)$$

On the other hand, from

$$\bar{H}^2 \begin{pmatrix} \Psi_p^A(x) \\ \Psi_p^B(x) \end{pmatrix} = \bar{E}_p^2 \begin{pmatrix} \Psi_p^A(x) \\ \Psi_p^B(x) \end{pmatrix}, \quad (42)$$

we find a set of decoupled equations,

$$H_A \Psi_p^A(x) = (\bar{E}_p^2 + \bar{\gamma}^2) \Psi_p^A(x), \quad (43)$$

$$H_B \Psi_p^B(x) = (\bar{E}_p^2 + \bar{\gamma}^2) \Psi_p^B(x). \quad (44)$$

When we set

$$\phi_p^A = \Psi_p^A(x), \quad \phi_{p-1}^B = \Psi_p^B(x), \quad (45)$$

$$E_{p-1}^B = E_p^A = \bar{E}_p^2 + \bar{\gamma}^2, \quad (46)$$

Eq. (37) is satisfied. Hence, the SUSY algebra is satisfied. The SUSY partners are the wave functions on the A and B sites.

VI. EXPLICIT SOLUTIONS OF THE NON-HERMITIAN SSH MODEL

We next seek the explicit solutions of the non-Hermitian model (27). This can be performed by simplifying the function (26). When ξ is large, we can approximate the gap function by a linear function as

$$\Delta(x) = (\kappa\lambda/\xi)x, \quad (47)$$

where we set $x = 0$ at the interface. The Hamiltonian is given by

$$\bar{H} = \begin{pmatrix} i\bar{\gamma} & A^\dagger \\ A & -i\bar{\gamma} \end{pmatrix}, \quad (48)$$

or

$$\tilde{H} = \begin{pmatrix} i\gamma\chi - i\gamma & A^\dagger \\ A & -i\gamma \end{pmatrix}, \quad (49)$$

where

$$A \equiv (\kappa\lambda/\xi)x + \kappa\partial_x, \quad A^\dagger \equiv (\kappa\lambda/\xi)x - \kappa\partial_x. \quad (50)$$

The commutator of the SUSY operators is calculated as

$$[A, A^\dagger] = \alpha, \quad \text{with } \alpha \equiv 2\kappa^2\lambda/\xi. \quad (51)$$

The standard commutation relation of the annihilation and creation operators follows:

$$[b, b^\dagger] = 1, \quad (52)$$

in terms of the scaled operators b and b^\dagger defined by

$$A \equiv \sqrt{\alpha}b, \quad A^\dagger \equiv \sqrt{\alpha}b^\dagger. \quad (53)$$

Equations (43) and (44) are rewritten as

$$\begin{aligned} \alpha b^\dagger b \Psi_p^A &= (\bar{E}_p^2 + \bar{\gamma}^2) \Psi_p^A, \\ \alpha(1 + b^\dagger b) \Psi_p^B &= (\bar{E}_p^2 + \bar{\gamma}^2) \Psi_p^B. \end{aligned} \quad (54)$$

These are solved as

$$\Psi_p^A(x) = h_p^A \langle x|p\rangle, \quad \Psi_p^B(x) = h_p^B \langle x|p-1\rangle, \quad (55)$$

$$\bar{E}_p^2 = -\bar{\gamma}^2 + \alpha p \quad (56)$$

for $p \geq 1$, where h_p^A and h_p^B are c numbers, $|p\rangle$ stands for the p th eigenfunction and $\langle x|p\rangle$ is its coordinate space representation. For $p = 0$, we have $E_0 = i\bar{\gamma}$, and the wave functions are given by the non-Hermitian JR solutions (30) and (31).

We note that the energy \bar{E}_p of the p th level is pure imaginary when

$$p < \frac{\bar{\gamma}^2}{\alpha} = \frac{\gamma \chi \xi}{4\kappa^2 \lambda}. \quad (57)$$

We call mode $|p\rangle$ the SUSY JR mode because we create it from the JR mode $|0\rangle$ by the operation of b^\dagger . The SUSY JR modes are supersymmetric, whereas the JR mode breaks it. They describe the numerically obtained energy spectrum shown in Figs. 2(b2)–2(d2).

We determine the relation between two c numbers h_p^A and h_p^B . We write down the eigenvalue equations (27) explicitly,

$$i\bar{\gamma}\Psi_p^A + A^\dagger\Psi_p^B = \bar{E}_p\Psi_p^A, \quad A\Psi_p^A - i\bar{\gamma}\Psi_p^B = \bar{E}_p\Psi_p^B, \quad (58)$$

which we rewrite with the use of (55) as

$$i\bar{\gamma}h_p^A|p\rangle + \sqrt{\alpha}h_p^B b^\dagger|p-1\rangle = \bar{E}_p h_p^A|p\rangle, \quad (59)$$

$$\sqrt{\alpha}h_p^A b|p\rangle - i\bar{\gamma}h_p^B|p-1\rangle = \bar{E}_p h_p^B|p-1\rangle. \quad (60)$$

It follows that

$$i\bar{\gamma}h_p^A + \sqrt{\alpha p}h_p^B = \bar{E}_p h_p^A, \quad (61)$$

$$\sqrt{\alpha p}h_p^A - i\bar{\gamma}h_p^B = \bar{E}_p h_p^B. \quad (62)$$

or

$$\sqrt{\alpha p}h_p^B = (\bar{E}_p - i\bar{\gamma})h_p^A, \quad (63)$$

$$\sqrt{\alpha p}h_p^A = (\bar{E}_p + i\bar{\gamma})h_p^B, \quad (64)$$

which leads to

$$h_p^B = \left(\frac{\bar{E}_p - i\bar{\gamma}}{\bar{E}_p + i\bar{\gamma}} \right)^{1/2} h_p^A. \quad (65)$$

Hence, the wave-function Ψ_p^B is determined once the wave-function Ψ_p^A is given.

Here we recall that there are two series of eigenfunctions corresponding to $\bar{E}_p^\pm = \pm\sqrt{-\bar{\gamma}^2 + \alpha p}$ for $p \geq 1$ and $\bar{E}_0^+ = i\bar{\gamma}$. We focus on SUSY JR modes, where $\bar{\gamma}^2 > \alpha p$. In the parameter region with $\bar{\gamma}^2 \gg \alpha p$, we would expand $\bar{E}_p^\pm = \pm i\bar{\gamma} + \dots$. Then, we have

$$\left(\frac{h_p^B}{h_p^A} \right)^2 = \frac{\bar{E}_p^+ - i\bar{\gamma}}{\bar{E}_p^+ + i\bar{\gamma}} \ll 1 \quad \text{for } \bar{E}_p^+ = i\bar{\gamma} + \dots, \quad (66)$$

$$\left(\frac{h_p^B}{h_p^A} \right)^2 = \frac{\bar{E}_p^- - i\bar{\gamma}}{\bar{E}_p^- + i\bar{\gamma}} \gg 1 \quad \text{for } \bar{E}_p^- = -i\bar{\gamma} + \dots. \quad (67)$$

Hence,

$$|\Psi_p^A| \gg |\Psi_p^B| \quad \text{for the series } \bar{E}_p^+, \quad (68)$$

$$|\Psi_p^A| \ll |\Psi_p^B| \quad \text{for the series } \bar{E}_p^-. \quad (69)$$

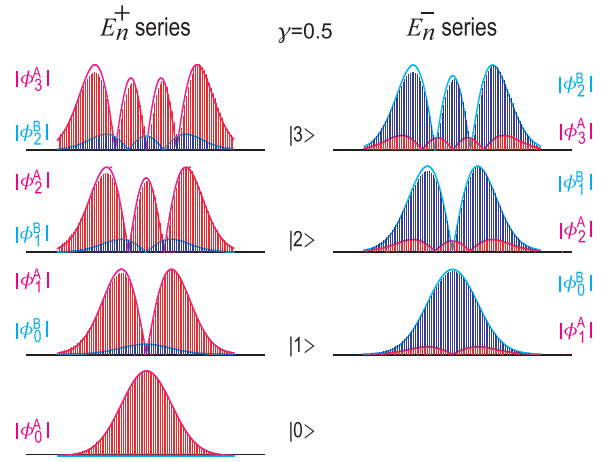


FIG. 6. Red (blue) bars show the amplitudes numerically calculated at the A (B) site. Magenta (cyan) heavy curves are analytical results given by Eq. (73), which envelop the numerical results very well. Each panel contains SUSY partners made of amplitudes $|\phi_n^A|$ and $|\phi_{n-1}^B|$. Their magnitudes are quite different for $\gamma = 0.5$. The left (right) column is for the series of the energy \bar{E}_n^+ (\bar{E}_n^-).

This explains a huge difference numerically found between the amplitudes at the A and B sites in Fig. 6.

We comment on the SUSY quantum mechanics. First of all, there are two series of energies $\bar{E}_p^\pm = \pm\sqrt{-\bar{\gamma}^2 + \alpha p}$, although the relevant energies are $E_{p-1}^B = E_p^A = \alpha p$ for both series in SUSY quantum mechanics. However, the magnitudes of the amplitudes are very different,

$$|\phi_p^A| \gg |\phi_{p-1}^B| \quad \text{for the series } \bar{E}_p^+, \quad (70)$$

$$|\phi_p^A| \ll |\phi_{p-1}^B| \quad \text{for the series } \bar{E}_p^-, \quad (71)$$

which follows from (45) and (69). These two series are shown in Fig. 6.

The wave function is given by $\langle x|p\rangle$ apart from the normalization constant, and, hence, it is written in terms of the Hermite polynomials precisely as in the Hermitian model,

$$\Psi_p^A(x) = h_p^A \sqrt{\frac{1}{p!2^p}} \sqrt{\frac{\lambda}{\pi\xi}} H_p \left(\sqrt{\frac{\lambda}{\xi}} x \right) \exp \left[-\frac{\lambda}{2\xi} x^2 \right], \quad (72)$$

$$\Psi_p^B(x) = h_p^B \Psi_{p-1}^A(x), \quad (73)$$

where h_p^B is given by Eq. (65) whereas h_p^A is to be determined numerically.

There is the JR mode only for the A site, whose wave functions are

$$\Psi_0^A(x) = h_0^A \exp \left[-\frac{\lambda}{2\xi} x^2 \right], \quad \Psi_0^B(x) = 0. \quad (74)$$

This is the SUSY-broken state.

Finally, we compare the analytic solutions and the numerical solutions of the wave functions in Fig. 6. The coincidence is very well between the analytic solution and the numerical results except for a minor difference where the mirror symmetry is slightly broken in the numerical results. It is due to the difference between the hopping parameters $\kappa_{A,n}$ and κ_B

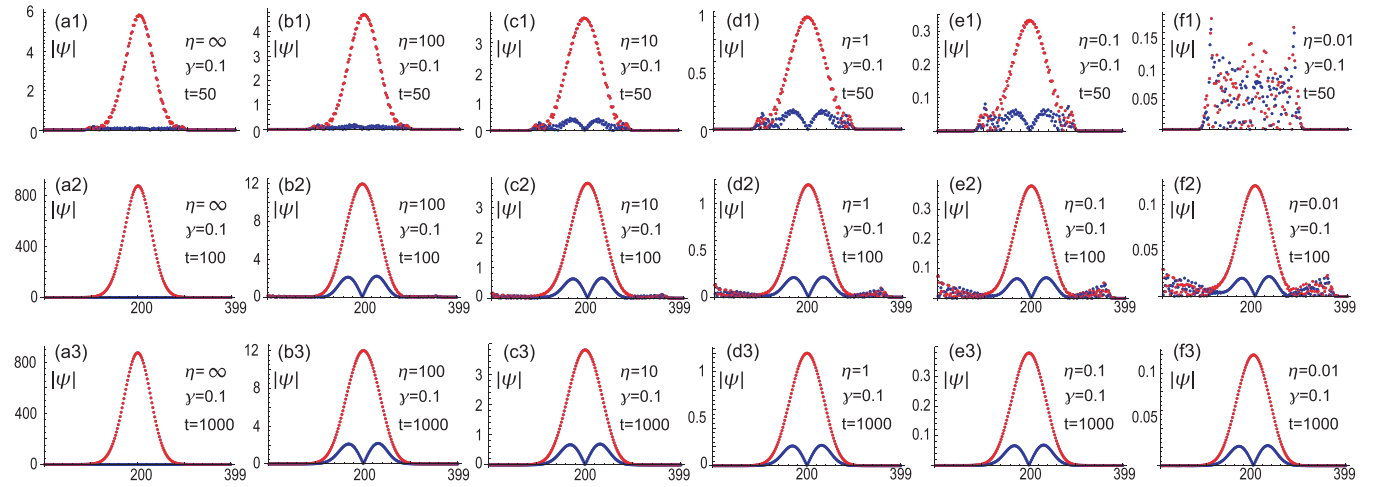


FIG. 7. Spatial profile of the amplitude $|\psi_n|$. (a1)–(a3) linear model, (b1)–(b3) $\eta = 100$, (c1)–(c3) $\eta = 10$, (d1)–(d3) $\eta = 1$, (e1)–(e3) $\eta = 0.1$, and (f1)–(f3) $\eta = 0.01$. We have set $\chi = 2$, $\gamma = 0.1$, $L = 399$, and $\xi = 200$. (a1)–(f1) $t = 50$, (a2)–(f2) $t = 100$, and (a3)–(f3) $t = 1000$. The wave function is saturated and fixed real at the A sites in red and pure imaginary at the B sites in blue for finite η .

in Eq. (3) where the band widths are different between the topological and trivial phases. This difference is taken care of in the numerical calculation but ignored in the analytical study.

VII. GAIN WITH SATURATION

A. Quench dynamics

We have so far studied the linear model containing loss and gain. The amplitude increases infinitely as time passes. Actually, there must be a saturation effect in gain, which makes the amplitude finite. We include the saturation effect by keeping η finite in Eq. (1). We show the results in Figs. 4(c1)–4(c3). The amplitudes remain finite due to the saturation effect. It is a topological interface laser stabilized by nonlinear and non-Hermiticity effects. We also show the time evolution of the amplitude $|\psi_{nT}|$ in Fig. 4(c4).

We show the spatial profile of the amplitude $|\psi_n|$ at $t = 50, 100, 1000$ for various η 's in Fig. 7. Main excitations are localized at the A sites in the vicinity of the interface, whose wave function is real. This is simply because the gain is given to the A sites. However, there are also excitations at the B sites as in Fig. 7, which is a nonlinearity effect. We observe three key properties: (1) Ψ^A is proportional to $\sqrt{\eta}$. (2) Ψ^B/Ψ^A is independent of η . (3) Ψ^B is pure imaginary, and it vanishes at the interface site. We explain them analytically based on the nonlinear JR theory in the following subsection.

There is an important remark. Bulk excitations emerge in transient states as in Figs. 7(b1)–7(f1) and 7(d2)–7(f2), but they disappear after enough time ($t = 1000$) as in Figs. 7(a3)–7(f3). The time for saturation is longer for smaller η . Hence, we conclude a stable single-mode topological lasing after enough time irrespective of the saturation parameter η .

B. Nonlinear Jackiw-Rebbi theory

We have numerically revealed the excitations at the B sites in the presence of the saturation term. We now show that they form the JR mode generalized to the nonlinear regime.

Replacing the linear gain term with the nonlinear gain term in Eq. (49), we have

$$\begin{pmatrix} \frac{i\gamma\chi}{1+|\Psi_A(x)|^2/\eta} - i\gamma & A^\dagger \\ A & -i\gamma \end{pmatrix} \begin{pmatrix} \Psi_A(x) \\ \Psi_B(x) \end{pmatrix} = E \begin{pmatrix} \Psi_A(x) \\ \Psi_B(x) \end{pmatrix}. \quad (75)$$

We analyze a small excitation at the B sites. Using a mean-field approximation, we obtain $\Psi_A(x)$ and $\Psi_B(x)$ as

$$\Psi_A(x) = c \exp\left[-\frac{\kappa\lambda}{2\xi}(1+c_2)x^2\right], \quad (76)$$

$$\Psi_B(x) = -ic \frac{x}{\eta} \frac{c_2\kappa\lambda}{\xi} \exp\left[-\frac{\kappa\lambda}{2\xi}(1+c_2)x^2\right], \quad (77)$$

where c is a normalization constant, and

$$c_2 = \frac{\gamma^2\chi^2\xi}{\kappa^2\lambda} \left[\frac{1}{1+|\bar{\Psi}_A|^2/\eta} - \frac{1}{1+|\Psi_A(0)|^2/\eta} \right], \quad (78)$$

with $\bar{\Psi}_A$ the mean of $\Psi_A(x)$. See Appendix B for a detailed derivation. We note that

$$\frac{\Psi_B(x)}{\Psi_A(x)} = -ix \frac{\gamma^2\chi^2}{\kappa} \left[\frac{1}{1+|\bar{\Psi}_A|^2/\eta} - \frac{1}{1+|\Psi_A(0)|^2/\eta} \right]. \quad (79)$$

The relative phases between A and B are fixed to be $\pm i$.

We summarize the key properties of the wave function. The equation of motion (75) becomes free from the parameter η if we scale the amplitudes by the factor $\sqrt{\eta}$ as we already noted in the paragraph below Eq. (6). It explains that $\Psi_A(x)$ is proportional to $\sqrt{\eta}$. Then, it follows from Eq. (79) that $\Psi_B(x)/\Psi_A(x)$ is independent of η . Equation (79) itself says

that $\Psi_B(x)$ is pure imaginary, and it vanishes at the interface site.

VIII. CONCLUSION AND DISCUSSION

We have explored the SSH model with a topological interface as a model of a large area single-mode laser. In previous works [27,30], the gain terms were only introduced at the edge sites in order to excite the topological edge states. On the contrary, in the present model, the gain terms are introduced to all the A sites. Although bulk modes are excited in transient process, they decay after enough time. The topological interface mode lases solely, which is the JR mode.

There are some eminent features with respect to the mode excitations. First, as a nonlinear effect, the JR mode has amplitudes not only at the A sites, but also at the B sites. Second, their relative phase is fixed and, hence, the JR mode presents a single coherent mode. Third, the A -site component of the JR mode is compatible with the gain terms introduced only to the A sites.

We have also revealed that SUSY quantum mechanics underlies the basic structure of the present bipartite system. By extending SUSY quantum mechanics to non-Hermitian systems, we have found a series of analytic solutions formed either A or B sites. They have pure imaginary energies and their wave functions are given by those of a harmonic oscillator. They form the SUSY partners where the JR state is the SUSY breaking state formed on the A sites. Furthermore, we have derived an analytic form of the JR mode in nonlinear regime by using a mean-field approximation.

We have applied quench dynamics to investigate a topological interface laser. However, it may be hard to observe the time evolution in actual optical experiments because the timescale is too short. The same physics is executed by the coupled-wave-guide arrays along the z direction [63], simply by replacing time t by coordinate z in the equation of motion.

We have developed an analysis based on the basic equation (1). On the other hand, it is well known that the dynamics of a laser is described by the rate equations. It is actually possible to derive Eq. (1) from the rate equations in a certain limit provided the carrier population is saturated. See details for Appendix C.

ACKNOWLEDGMENTS

M.E. was supported by CREST, JST (Grant No. JP-MJCR20T2). N.I. was supported by the Grants-in-Aid for Scientific Research from MEXT KAKENHI (Grant. No. JP21J40088). Y.O. was supported by the Grants-in-Aid for Scientific Research from MEXT KAKENHI (Grants No. 22H01994 and No. 22H00298). S.I. was supported by CREST, JST (Grant No. JPMJCR19T1) and the Grants-in-Aid for Scientific Research from MEXT KAKENHI (Grants No. 22H00298 and No. 22H01994).

APPENDIX A: TOPOLOGICAL PROPERTY OF THE NON-HERMITIAN SSH MODEL

We consider a homogeneous system. The Hamiltonian in the momentum space corresponding to the hopping matrix

(9) is

$$\begin{aligned} \tilde{H} &= \begin{pmatrix} -i\gamma(1-\chi) & \kappa_A + \kappa_B e^{-iak} \\ \kappa_A + \kappa_B e^{iak} & -i\gamma \end{pmatrix}, \\ &= -i\gamma \left(1 - \frac{\chi}{2}\right) I_2 + \bar{H}_{\text{SSH}}, \end{aligned} \quad (\text{A1})$$

with a as the lattice constant and

$$\bar{H} \equiv \begin{pmatrix} i\gamma\chi/2 & \kappa_A + \kappa_B e^{-iak} \\ \kappa_A + \kappa_B e^{iak} & -i\gamma\chi/2 \end{pmatrix}. \quad (\text{A2})$$

The Hamiltonian \bar{H}_{SSH} is non-Hermitian for $\gamma \neq 0$. The relation between the eigenenergy of the Hamiltonians (A1) and (A2) is

$$\tilde{E} = -i\gamma \left(1 - \frac{\chi}{2}\right) + \bar{E}_{\text{SSH}}. \quad (\text{A3})$$

The energy spectrum reads

$$\bar{E}(k) = \pm \sqrt{\kappa_A^2 + \kappa_B^2 + 2\kappa_A\kappa_B \cos ak - \gamma^2}. \quad (\text{A4})$$

Especially, we have

$$\bar{E}(\pi/a) = \pm \sqrt{(\kappa_A - \kappa_B)^2 - \gamma^2}. \quad (\text{A5})$$

The system is the PT preserved phase for $\gamma < |\kappa_A - \kappa_B|$ where the bulk energy is real even though the system is non-Hermitian, whereas the system is the PT-broken phase for $\gamma > |\kappa_A - \kappa_B|$, where the bulk energy becomes pure imaginary for a certain range of the momentum k .

We recall that the PT-symmetry operation is defined by

$$\text{PT} = \sigma_x K, \quad (\text{A6})$$

with K as the complex conjugation. Since we have

$$\text{PT} \bar{H}(k) \text{PT}^{-1} = \bar{H}(k), \quad (\text{A7})$$

and, hence, \bar{H}_{SSH} is a PT-symmetric Hamiltonian.

The topological number is defined with respect to the Hamiltonian (A2). We define the right and left eigenvectors by

$$H|\psi^R\rangle = E|\psi^R\rangle, \quad H^\dagger|\psi^L\rangle = E|\psi^L\rangle. \quad (\text{A8})$$

The non-Hermitian Zak phase is a topological number [64],

$$W \equiv \frac{i}{2\pi/a} \int_0^{2\pi/a} \langle \psi^L | \frac{\partial}{\partial k} | \psi^R \rangle dk. \quad (\text{A9})$$

It is straightforward to show that $W = 1$ for $\kappa_A < \kappa_B$ and $W = 0$ for $\kappa_A > \kappa_B$ irrespective of γ . Hence, the system is topological for $\kappa_A < \kappa_B$ and trivial for $\kappa_A > \kappa_B$.

APPENDIX B: NONLINEAR JACKIW-REBBI SOLUTION

We derive a set of the saturated distribution (76) and (77) from Eq. (75). First, we write Eq. (75) explicitly as

$$i\gamma \left(\frac{\chi}{1 + |\Psi_A(x)|^2/\eta} - 1 \right) \Psi_A(x) + A^\dagger \Psi_B(x) = E \Psi_A(x), \quad (\text{B1})$$

$$A \Psi_A(x) - i\gamma \Psi_B(x) = E \Psi_B(x), \quad (\text{B2})$$

where A and A^\dagger are given by Eq. (25) with Eq. (26). The second equation is solved as

$$\Psi_B(x) = \frac{A\Psi_A(x)}{E + i\gamma}, \quad (\text{B3})$$

which we insert into the first equation to derive

$$A^\dagger A\Psi_A(x) = (E + i\gamma) \left[E - i\gamma \left(\chi \frac{1}{1 + |\Psi_A(x)|^2/\eta} - 1 \right) \right] \times \Psi_A(x). \quad (\text{B4})$$

We assume that the energy is modified from Eq. (14) as

$$E = i\gamma(\chi - 1) + c_1, \quad (\text{B5})$$

where c_1 is a constant to be determined. Inserting it and we have

$$A^\dagger A\Psi_A(x) \simeq i\gamma\chi \left[c_1 + i\gamma\chi \left(1 - \frac{1}{1 + |\Psi_A(0)|^2/\eta} \right) \right] \Psi_A(x),$$

where we have used an approximation $|\Psi_A(x)|^2 \simeq |\Psi_A(0)|^2$ because $\Psi_A(x)$ rapidly decreases except at $x = 0$. We choose

$$c_1 = i\gamma\chi \left(\frac{1}{1 + |\bar{\Psi}_A|^2/\eta} - 1 \right), \quad (\text{B6})$$

where $\bar{\Psi}_A$ is the mean value of $\Psi_A(x)$. We obtain

$$A^\dagger A\Psi_A(x) = -\gamma^2\chi^2 \left[\frac{1}{1 + |\bar{\Psi}_A|^2/\eta} - \frac{1}{1 + |\Psi_A(0)|^2/\eta} \right] \times \Psi_A(x). \quad (\text{B7})$$

On the other hand, we assume a wave function modified from Eq. (74) as

$$\Psi_A(x) = c \exp \left[-\frac{\kappa\lambda}{2\xi} (1 + c_2)x^2 \right], \quad (\text{B8})$$

where c is a normalization constant and c_2 is a constant to be determined. Applying A and $A^\dagger A$ to $\Psi_A(x)$, we obtain

$$A\Psi_A(x) \simeq -\frac{c_2\kappa\lambda}{\xi} x\Psi_A(x), \quad (\text{B9})$$

$$A^\dagger A\Psi_A(x) \simeq \frac{c_2\kappa^2\lambda}{\xi} \Psi_A(x). \quad (\text{B10})$$

Comparing (B10) with Eq. (B7), we obtain

$$c_2 = \frac{\gamma^2\chi^2\xi}{\kappa^2\lambda} \left[\frac{1}{1 + |\bar{\Psi}_A|^2/\eta} - \frac{1}{1 + |\Psi_A(0)|^2/\eta} \right]. \quad (\text{B11})$$

With the use of Eqs. (B3) and (B9), $\Psi_B(x)$ is derived as

$$\Psi_B(x) = -icx \frac{c_2\kappa\lambda}{\xi} \exp \left[-\frac{\kappa\lambda}{2\xi} (1 + c_2)x^2 \right]. \quad (\text{B12})$$

It is the saturated distribution (77) in the main text. We then have

$$\frac{\Psi_B(x)}{\Psi_A(x)} = -ix \frac{\gamma^2\chi^2}{\kappa} \left[\frac{1}{1 + |\bar{\Psi}_A|^2/\eta} - \frac{1}{1 + |\Psi_A(0)|^2/\eta} \right], \quad (\text{B13})$$

which is Eq. (79) in the main text.

APPENDIX C: RATE EQUATION

The rate equations read [28,37,65]

$$\frac{dE_n^A}{dt} = \frac{1}{2} \left[-\gamma_0 + \sigma(N_n^A - 1) \right] \times (1 - i\alpha_H)E_n^A + i\kappa_A^0 E_n^B + i\kappa_B^0 E_{n-1}^B, \quad (\text{C1})$$

$$\frac{dE_n^B}{dt} = \frac{1}{2} \left[-\gamma_0 + \sigma(N_n^B - 1) \right] \times (1 - i\alpha_H)E_n^B + i\kappa_A^0 E_n^A + i\kappa_B^0 E_{n+1}^A, \quad (\text{C2})$$

$$\frac{dN_n^A}{dt} = R_A - \frac{N_n^A}{\tau_r} - F(N_n^A - 1)|E_n^A|^2, \quad (\text{C3})$$

$$\frac{dN_n^B}{dt} = R_B - \frac{N_n^B}{\tau_r} - F(N_n^B - 1)|E_n^B|^2, \quad (\text{C4})$$

where E_n^A and E_n^B are electric-field amplitudes in sublattices A and B and N_n^A and N_n^B are carrier population densities.

We assume the carrier is saturated

$$\frac{dN_n^A}{dt} = 0, \quad \frac{dN_n^B}{dt} = 0, \quad (\text{C5})$$

or

$$N_n^A - 1 = \frac{F|E_n^A|^2 + R_A}{F|E_n^A|^2 + 1/\tau_r} - 1 = \frac{R_A - 1/\tau_r}{F|E_n^A|^2 + 1/\tau_r}, \quad (\text{C6})$$

$$N_n^B - 1 = \frac{F|E_n^B|^2 + R_B}{F|E_n^B|^2 + 1/\tau_r} - 1 = \frac{R_B - 1/\tau_r}{F|E_n^B|^2 + 1/\tau_r}. \quad (\text{C7})$$

By inserting them into the rate equations, we have

$$\frac{dE_n^A}{dt} = \frac{1}{2} \left[-\gamma_0 + \sigma \frac{R_A - 1/\tau_r}{F|E_n^A|^2 + 1/\tau_r} \right] \times (1 - i\alpha_H)E_n^A + i\kappa_A^0 E_n^B + i\kappa_B^0 E_{n-1}^B, \quad (\text{C8})$$

$$\frac{dE_n^B}{dt} = \frac{1}{2} \left[-\gamma_0 + \sigma \frac{R_B - 1/\tau_r}{F|E_n^B|^2 + 1/\tau_r} \right] \times (1 - i\alpha_H)E_n^B + i\kappa_A^0 E_n^A + i\kappa_B^0 E_{n+1}^A, \quad (\text{C9})$$

or

$$i \frac{dE_n^A}{dt} = \frac{i}{2} \left[-\gamma_0 + \sigma \frac{\tau_r R_A - 1}{1 + \tau_r F|E_n^A|^2} \right] \times (1 - i\alpha_H)E_n^A - \kappa_A^0 E_n^B - \kappa_B^0 E_{n-1}^B, \quad (\text{C10})$$

$$i \frac{dE_n^B}{dt} = \frac{i}{2} \left[-\gamma_0 + \sigma \frac{\tau_r R_B - 1}{1 + \tau_r F|E_n^B|^2} \right] \times (1 - i\alpha_H)E_n^B - \kappa_A^0 E_n^A - \kappa_B^0 E_{n+1}^A. \quad (\text{C11})$$

When α_H is negligible and $\tau_r R_B = 1$, by setting

$$\psi_n^A = E_n^A, \quad \psi_n^B = E_n^B, \quad \kappa_A = -\kappa_A^0, \quad \kappa_B = -\kappa_B^0, \quad (\text{C12})$$

$$\gamma = -\gamma_0/2, \quad \eta = \tau_r F, \quad \gamma\chi = \sigma(\tau_r R_A - 1), \quad (\text{C13})$$

they are reduced to Eq. (1) in the main text.

- [1] M. Z. Hasan and C. L. Kane, *Rev. Mod. Phys.* **82**, 3045 (2010).
- [2] X.-L. Qi and S.-C. Zhang, *Rev. Mod. Phys.* **83**, 1057 (2011).
- [3] W. P. Su, J. R. Schrieffer, and A. J. Heeger, *Phys. Rev. Lett.* **42**, 1698 (1979).
- [4] A. B. Khanikaev, S. H. Mousavi, W.-K. Tse, M. Kargarian, A. H. MacDonald, and G. Shvets, *Nature Mater.* **12**, 233 (2013).
- [5] M. Hafezi, E. Demler, M. Lukin, and J. Taylor, *Nat. Phys.* **7**, 907 (2011).
- [6] M. Hafezi, S. Mittal, J. Fan, A. Migdall, and J. Taylor, *Nat. Photonics* **7**, 1001 (2013).
- [7] L. H. Wu and X. Hu, *Phys. Rev. Lett.* **114**, 223901 (2015).
- [8] L. Lu, J. D. Joannopoulos and M. Soljacic, *Nat. Photonics* **8**, 821 (2014).
- [9] T. Ozawa, H. M. Price, N. Goldman, O. Zilberberg, and I. Carusotto, *Phys. Rev. A* **93**, 043827 (2016).
- [10] D. Leykam and Y. D. Chong, *Phys. Rev. Lett.* **117**, 143901 (2016).
- [11] A. B. Khanikaev and G. Shvets, *Nat. Photonics* **11**, 763 (2017).
- [12] X. Zhou, Y. Wang, D. Leykam, and Y. D. Chong, *New J. Phys.* **19**, 095002 (2017).
- [13] T. Ozawa, H. M. Price, A. Amo, N. Goldman, M. Hafezi, L. Lu, M. C. Rechtsman, D. Schuster, J. Simon, O. Zilberberg, and L. Carusotto, *Rev. Mod. Phys.* **91**, 015006 (2019).
- [14] Y. Ota, F. Liu, R. Katsumi, K. Watanabe, K. Wakabayashi, Y. Arakawa, and S. Iwamoto, *Optica* **6**, 786 (2019).
- [15] T. Ozawa and H. M. Price, *Nat. Rev. Phys.* **1**, 349 (2019).
- [16] A. E. Hassan, F. K. Kunst, A. Moritz, G. Andler, E. J. Bergholtz, and M. Bourennane, *Nat. Photonics* **13**, 697 (2019).
- [17] Y. Ota, K. Takata, T. Ozawa, A. Amo, Z. Jia, B. Kante, M. Notomi, Y. Arakawa, and S. Iwamoto, *Nanophotonics* **9**, 547 (2020).
- [18] M. Li, D. Zhirihin, D. Filonov, X. Ni, A. Slobozhanyuk, A. Alu, and A. B. Khanikaev, *Nat. Photonics* **14**, 89 (2020).
- [19] H. Yoshimi, T. Yamaguchi, Y. Ota, Y. Arakawa, and S. Iwamoto, *Opt. Lett.* **45**, 2648 (2020).
- [20] M. Kim, Z. Jacob, and J. Rho, *Light: Sci. Appl.* **9**, 130 (2020).
- [21] S. Iwamoto, Y. Ota, and Y. Arakawa, *Opt. Mater. Express* **11**, 319 (2021).
- [22] L. Feng, R. El-Ganainy, and L. Ge, *Nat. Photonics* **11**, 752 (2017).
- [23] R. El-Ganainy, K. G. Makris, M. Khajavikhan, Z. H. Musslimani, S. Rotter, and D. N. Christodoulides, *Nat. Phys.* **14**, 11 (2018).
- [24] L. Pilozzi and C. Conti, *Phys. Rev. B* **93**, 195317 (2016).
- [25] B. Bahari, A. Ndao, F. Vallini, A. El Amili, Y. Fainman, and B. Kante, *Science* **358**, 636 (2017).
- [26] G. Harari, M. A. Bandres, Y. Lumer, M. C. Rechtsman, Y. D. Chong, M. Khajavikhan, D. N. Christodoulides, M. Segev, *Science* **359**, eaar4003 (2018).
- [27] M. A. Bandres, S. Wittek, G. Harari, M. Parto, J. Ren, M. Segev, D. N. Christodoulides, and M. Khajavikhan, *Science* **359**, eaar4005 (2018).
- [28] S. Longhi, Y. Kominis, and V. Kovanis, *Europhys. Lett.* **122**, 14004 (2018).
- [29] S. K. Ivanov, Y. Zhang, Y. V. Kartashov, and D. V. Skryabin, *APL Photonics* **4**, 126101 (2019).
- [30] Y. V. Kartashov and D. V. Skryabin, *Phys. Rev. Lett.* **122**, 083902 (2019).
- [31] Y. Zeng, U. Chattopadhyay, B. Zhu, B. Qiang, J. Li, Y. Jin, L. Li, A. G. Davies, E. H. Linfield, B. Zhang, Y. Chong, and Q. J. Wang, *Nature (London)* **578**, 246 (2020).
- [32] H. Zhong, Y. Li, D. Song, Y. V. Kartashov, Y. Zhang, Y. Zhang, and Z. Chen, *Laser Photon. Rev.* **14**, 2000001 (2020).
- [33] H. Schomerus, *Opt. Lett.* **38**, 1912 (2013).
- [34] S. Weimann, M. Kremer, Y. Plotnik, Y. Lumer, S. Nolte, K. G. Makris, M. Segev, M. C. Rechtsman, and A. Szameit, *Nature Mater.* **16**, 433 (2017).
- [35] P. St-Jean, V. Goblot, E. Galopin, A. Lemaitre, T. Ozawa, L. Le Gratiet, I. Sagnes, J. Bloch, and A. Amo, *Nat. Photonics* **11**, 651 (2017).
- [36] Y. Ota, R. Katsumi, K. Watanabe, S. Iwamoto, and Y. Arakawa, *Commun. Phys.* **1**, 86 (2018).
- [37] M. Parto, S. Wittek, H. Hodaei, G. Harari, M. A. Bandres, J. Ren, M. C. Rechtsman, M. Segev, D. N. Christodoulides, and M. Khajavikhan, *Phys. Rev. Lett.* **120**, 113901 (2018).
- [38] H. Zhao, P. Miao, M. H. Teimourpour, S. Malzard, R. El-Ganainy, H. Schomerus, and L. Feng, *Nat. Commun.* **9**, 981 (2018).
- [39] S. Malzard and H. Schomerus, *New J. Phys.* **20**, 063044 (2018).
- [40] S. Malzard, E. Cancellieri, and H. Schomerus, *Opt. Express* **26**, 22506 (2018).
- [41] H. Zhong, Y. V. Kartashov, A. Szameit, Y. Li, C. Liu, and Y. Zhang, *APL Photonics* **6**, 040802 (2021).
- [42] M. Yoshida *et al.*, *Nature Mater.* **18**, 121 (2019).
- [43] S.-L. Chua, L. Lu, J. Bravo-Abad, J. D. Joannopoulos, and M. Soljačić, *Opt. Lett.* **39**, 2072 (2014).
- [44] R. Contractor *et al.*, *Nature (London)* **608**, 692 (2022).
- [45] X. Gao *et al.*, *Nat. Nanotechnol.* **15**, 1012 (2020).
- [46] L. Yang *et al.*, *Nat. Photonics* **16**, 279 (2022).
- [47] N. Ishida, Y. Ota, W. Lin, and T. Byrnes, Y. Arakawa, and S. Iwamoto, *Nanophotonics* **11**, 2169 (2022).
- [48] R. Jackiw and C. Rebbi, *Phys. Rev. D* **13**, 3398 (1976).
- [49] M. Ezawa, *J. Phys. Soc. Jpn.* **91**, 024703 (2022).
- [50] M. Ezawa, *J. Phys. Soc. Jpn.* **90**, 114605 (2021).
- [51] M. Ezawa, *Phys. Rev. B* **104**, 235420 (2021).
- [52] M. Ezawa, *Phys. Rev. Res.* **4**, 013195 (2022).
- [53] E. Witten, *Nucl. Phys. B* **188**, 513 (1981); **202**, 253 (1982).
- [54] F. Cooper, A. Khare, and U. Sukhatme, *Phys. Rep.* **251**, 267 (1995).
- [55] F. Cooper, A. Khare, and U. Sukhatme, *Supersymmetry in Quantum Mechanics* (World Scientific, Singapore, 2001).
- [56] G. Junker, *Supersymmetric Methods in Quantum and Statistical Physics* (Springer, Berlin, 1996).
- [57] M. Heinrich, M. A. Miri, S. Stuzer, R. El-Ganainy, S. Nolte, A. Szameit, and D. N. Christodoulides, *Nat. Commun.* **5**, 3698 (2014).
- [58] M.-A. Miri, M. Heinrich, R. El-Ganainy, and D. N. Christodoulides, *Phys. Rev. Lett.* **110**, 233902 (2013).
- [59] R. El-Ganainy, Li Ge, M. Khajavikhan, and D. N. Christodoulides, *Phys. Rev. A* **92**, 033818 (2015).
- [60] M. P. Hokmabadi, N. S. Nye, R. El-Ganainy, D. N. Christodoulides, and M. Khajavikhan, *Science* **363**, 623 (2019).

- [61] B. Midya, H. Zhao, X. Qiao, P. Miao, W. Walasik, Z. Zhang, N. M. Litchinitser, and L. Feng, [Photonic Res.](#) **7**, 363 (2019).
- [62] X. Qiao, B. Midya, Z. Gao, Z. Zhang, H. Zhao, T. Wu, J. Yim, R. Agarwal, N. M. Litchinitser, and L. Feng, [Science](#) **372**, 403 (2021).
- [63] S. Longhi, [Laser Photon. Rev.](#) **3**, 243 (2009).
- [64] S. Lieu, [Phys. Rev. B](#) **97**, 045106 (2018).
- [65] A. U. Hassan, H. ei, M. A. Miri, M. Khajavikhan, and D. N. Christodoulides, [Phys. Rev. A](#) **92**, 063807 (2015).